



Research article

Cross-spectral iris recognition using phase-based matching and homomorphic filtering

Maulisa Oktiana^a, Takahiko Horiuchi^b, Keita Hirai^b, Khairun Saddami^a, Fitri Arnia^{a,c,d}, Yuwaldi Away^{a,c}, Khairul Munadi^{a,c,d,*}^a Graduate School of Engineering, Universitas Syiah Kuala, Banda Aceh, 23111, Indonesia^b Department of Imaging Sciences, Graduate School of Engineering, Chiba University, Chiba, 263-8522, Japan^c Department of Electrical and Computer Engineering, Universitas Syiah Kuala, Banda Aceh, 23111, Indonesia^d Telematics Research Center (TRC) Universitas Syiah Kuala, Banda Aceh, 23111, Indonesia

ARTICLE INFO

Keywords:

Biomedical engineering
Computer science
Electrical engineering
Medical imaging
Computer engineering
Signal processing
Image processing
Signal processing
Cross-spectral matching
Phase-based iris recognition
Band-limited phase-only correlation (BLPOC)
Phase-only correlation (POC)
Iris recognition

ABSTRACT

In cross-spectral iris recognition, different spectral bands are used to obtain rich information of the human iris. Previous studies on cross-spectral iris recognition are based primarily on feature-based approaches, which are prone to the changes in parameters in the feature extraction process, such as spatial position and iris image acquisition conditions. These parameters can degrade iris recognition performance. In this paper, we present a phase-based approach for cross-spectral iris recognition using phase-only correlation (POC) and band-limited phase-only correlation (BLPOC). A phase-based iris recognition system recognizes an iris using the phase information contained in the iris image; therefore, its performance is not affected by feature extraction parameters. However, the performance of a phase-based cross-spectral iris recognition is strongly influenced by specular reflection. Different illumination conditions may produce different iris images from the same subject. To overcome this challenge, we integrate a photometric normalization technique—homomorphic filtering—with phase-based cross-spectral iris recognition. The experimental results reveal that the proposed technique achieved an excellent matching performance with an equal error rate of 0.59% and a genuine acceptance rate of 95%.

1. Introduction

There has been a significant increase in the use of cross-spectral iris applications over the past several decades. Cross-spectral iris recognition has been developed to overcome the limitations of iris recognition in a single spectrum, such as visible (VIS) wavelength-based iris recognition [1, 2], and near-infrared (NIR) wavelength based iris recognition [3, 4]. Iris recognition in the cross-spectral domain is considered to be superior among same spectral iris recognition approaches, as the cross-spectral domain employs different spectral bands to obtain richer information of the human iris [5].

Recognition performance can be enhanced by using complementary iris information from different spectral bands; this leads to more discriminative recognition features [6]. Cross-spectral iris recognition has widespread use in various biometric applications, such as the national ID card system, biometric passports and visas, criminal investigations, and e-commerce [7, 8]. In addition, several imaging

products equipped with cameras from different spectral bands, such as Microsoft Kinect2, FLIR ONE, and Heatwave, are currently available on the market [9].

Iris recognition in the VIS spectrum is affected by reflection from the cornea; dark-colored irises are clearly visible, while light-colored irises are highlighted [10]. Meanwhile, the NIR spectrum disbands the striking patterns of the pigment melanin in the iris, and the iris recognition is affected by less reflections [11]. Consequently, recognition of iris images in both NIR and VIS spectra is more challenging than recognition within the same spectrum. Because NIR and VIS spectra are widely used and targeted in commercial implementations [12], the present study focuses on the NIR-VIS cross-spectral domain.

Existing studies on cross-spectral iris recognition primarily have a feature-based approach [13, 14, 15, 16, 17], which is significantly affected by parameters in the feature extraction process, such as spatial position and orientation, as well as iris image acquisition conditions that

* Corresponding author.

E-mail address: khairul.munadi@unsyiah.ac.id (K. Munadi).

can degrade recognition performance. To address these limitations, we propose cross-spectral iris recognition using the phase of NIR and VIS iris images. The principle of this approach involves using the phase component of the 2D discrete Fourier transformation (DFT) of NIR and VIS images to calculate the matching score. Phase-based iris recognition is simple yet effective due to the availability of important characteristics in the phase component of an image.

Phase-based image matching has been used in various biometric recognition tasks in the VIS spectrum, including fingerprint recognition [18, 19, 20, 21], palm print recognition [22], finger knuckle recognition [23], and iris recognition [24, 25]. In this study, we apply phase-based iris matching techniques to the cross-spectral domain. Figure 1 presents a simplified diagram of the phase-based cross-spectral iris matching. An image has a phase and amplitude; however, only the phase is used for matching purposes. In the phase-based matching, the most challenging task is to obtain a similar spectrum of the phase component between the two images.

Using images from different spectral bands results in a different spectrum of the phase component of each image, which may affect recognition performance. This problem can be attributed primarily to specular reflection caused by illumination variations in the two images. Therefore, we propose using a photometric normalization technique to address specular reflection. We explore different filtering techniques for integration into phase-based cross-spectral iris recognition, such as discrete cosine transform (DCT)-based filtering, TanTriggs filtering, and homomorphic filtering. In addition, in contrast to previous studies, this study considers the textural information contained in each color space (i.e. red, green, blue, Y, and V channels) to achieve more reliable recognition.

The main contributions of this paper are as follows:

- To the best our knowledge, this is the first study that employs phase-based iris matching in the cross-spectral domain. The phase information of iris images is obtained from the DFT spectrum of the NIR and VIS images. We address specular reflection using homomorphic filtering prior to the segmentation steps.
- In contrast to previous approaches, which perform matching mainly in the red channel of the VIS image, we use various color channels such as the green, blue, Y, and V channels of VIS iris images to obtain an improved representation of iris patterns.
- We significantly improve the performance of cross-spectral iris recognition by integrating phase-based matching and a photometric normalization technique known as homomorphic filtering.

The remainder of this paper is structured as follows. Section 2 describes the related works, while Section 3 outlines our proposed method.

Section 4 provides the experimental results and a discussion, and Section 5 presents conclusions.

2. Related work

Typical cross-spectral iris recognitions methods exploit feature-based correspondence, in which feature descriptors are used to build the feature vectors corresponding to a given iris image [26]. Metrics such as the Hamming distance and Euclidean distance are also used to compute the similarity between the iris templates. Feature-based cross-spectral iris matchings can be divided into three categories: structural matching, statistical matching, and block matching [27].

In structural matching, the corresponding pixels of NIR and VIS images are used to describe the structure of an iris pattern. Oktiana et al. [28] extracted iris texture using the multi-scale Weberface and Gabor local binary pattern (MGLBP) texture feature generator. Other authors explored the integration of texture features with various feature descriptors. Ramaiah and Kumar [29] convolved a 1-D log-Gabor filter with two local binary pattern (LBP) variants: four-patch LBP and three-patch LBP.

In statistical matching, the matching process is based on the statistical properties of the NIR and VIS iris images. Abdullah et al. [30] used binarized statistical image features (BSIF) to extract the statistical features of NIR and VIS iris images. BSIF features are able to represent the statistical properties of NIR and VIS iris images with high iris recognition performance.

Block matching was used by Vyas and Kanumuri [31], who performed block-based iris matching for surveillance applications. A 2D Gabor filter bank was used as the feature extraction method. With this method, an iris pattern was computed and divided into sub-blocks using the difference of variance (DoV) features at various scales and orientations. The resulting feature vectors were considerably compact and precise; however, the matching performance was strongly influenced by various parameters in the feature extraction process.

Wang and Kumar [32] proposed cross-spectral iris recognition using convolutional neural networks (CNNs). The CNN-based approach resulted in the compact representation of iris templates and was highly robust to nonlinear cross-spectral distortions. However, this technique had a limited ability to recognize poor-quality iris images caused by illumination variations between the NIR and VIS images, as in the PolyU Iris Database [33]. The limitations of the existing cross-spectral iris recognition methods are summarized in Table 1.

Although various cross-spectral iris recognition methods have been proposed, the majority of them have an equal error rate (EER) of greater than 5% [15], which is considered unsatisfactory performance. Thus, additional approaches are necessary for improving recognition

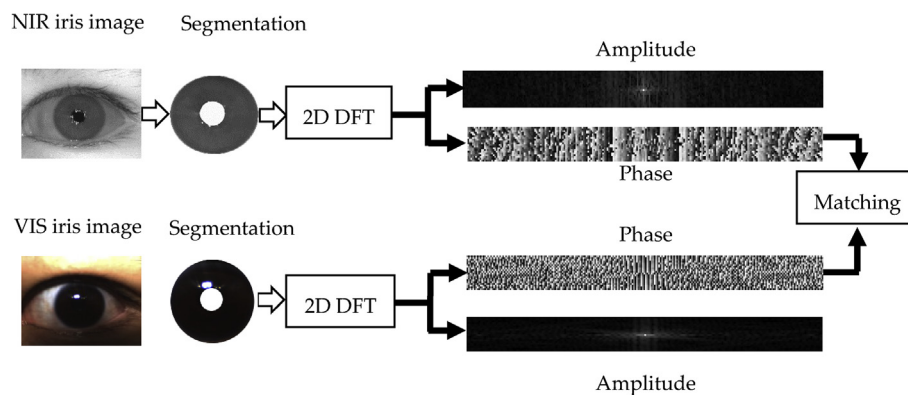


Figure 1. Simplified overview of the phase-based cross-spectral iris matching. The matching process is based on the phase component of the two dimensional (2D) discrete Fourier transform (DFT) of near-infrared (NIR) and visible (VIS) iris images. (iris image source: PolyU iris database [47]).

Table 1. Comparison of proposed and existing cross-spectral iris recognition methods.

Category	Methods	Similarity Measurement	Strength	Weakness
Structural matching	Multi-scale Weberface and Gabor local binary pattern (MGLBP) [28]	Hamming distance	Provides texture information of iris patterns	Performance of iris recognition is dependent on feature extraction parameters
Statistical matching	Binary statistical Image Feature, Difference of Gaussian, and Multi scale Weberface [30]	Hamming distance	Accommodates complementary features for the iris patterns	Cross-spectral illumination problems
Block matching	2D Gabor filter and the difference of variance (DoV) [31]	Manhattan distance	Extracts rich iris information from different scales and orientations	Not suitable for cross-spectral domain
Learning-based matching	Convolutional neural network (CNN) [32]	Hamming distance	Extracts efficient iris features using a large amount of training data	Limited ability to recognize given poor image quality

performance with an EER of less than 5%. Ito and Aoki [34] used phase-based matching, or phase-only correlation (POC), for fingerprint recognition in the VIS spectrum. Here, POC provided an excellent similarity measure for recognition, and was invariant to the translational displacement for image registration.

Miyazawa et al. [35] were among the first to use phase-based image matching for iris recognition in the VIS spectrum. In their study, the phase information contained the inherent features and characteristics of the iris, and their method resulted in an EER of 2.64 %. Motivated by the superior performance of the phase-based approach in the VIS spectrum, in this study, we used phase-based correlation to improve cross-spectral iris recognition performance and achieve an EER of less than 5%.

3. Proposed method

Figure 2 presents the proposed framework for cross-spectral iris recognition using phase-based correlation. In the proposed method, an NIR iris image was used for testing, while a VIS iris image was used for training. First, homomorphic filtering was performed for both the NIR and VIS iris images to reduce specular reflection. Then, the iris region was obtained through segmentation and normalization processes. The NIR iris template was then matched against the VIS iris template using the phase of the 2D DFT spectrum of the corresponding NIR and VIS

images. Finally, the matching decision was assessed with the EER and receiver operating characteristic (ROC) curve parameters. Each of the steps above is described in more detail below.

3.1. Filtering

Figure 3 presents iris images captured in the NIR and VIS spectra. The NIR iris images were visually similar to the VIS iris images; however, the information obtained from each wavelength differed. In the VIS image, the iris pattern was affected by specular reflection caused by frontal illumination. Thus, we first removed reflections in both the NIR and VIS iris images to obtain a similar representation of the iris pattern. Homomorphic filtering was used to correct non-uniform illumination in both images.

We employed the homomorphic filtering algorithm described in [36] as follows:

1. The NIR and VIS iris images (I_{in}) are transformed into the logarithmic domain (I_{log}):

$$I_{log} = \log(I_{in}) \tag{1}$$

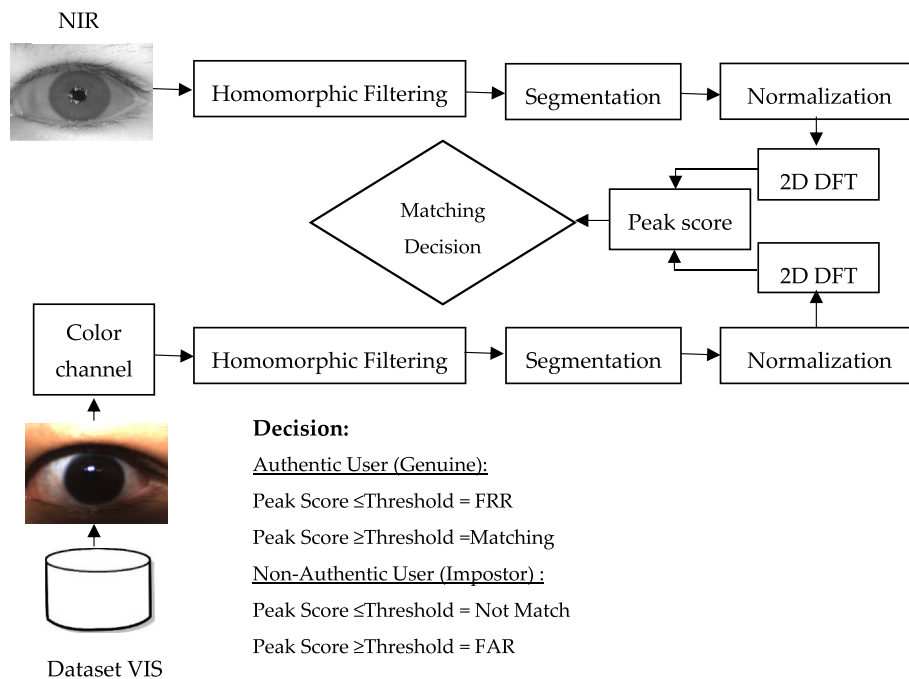


Figure 2. Proposed framework of cross-spectral iris recognition using phase-based image matching. NIR: near-infrared; VIS: visible; DFT: discrete Fourier transform; FRR: false rejection rate; FAR: false acceptance rate. (iris image source: PolyU iris database [47]).

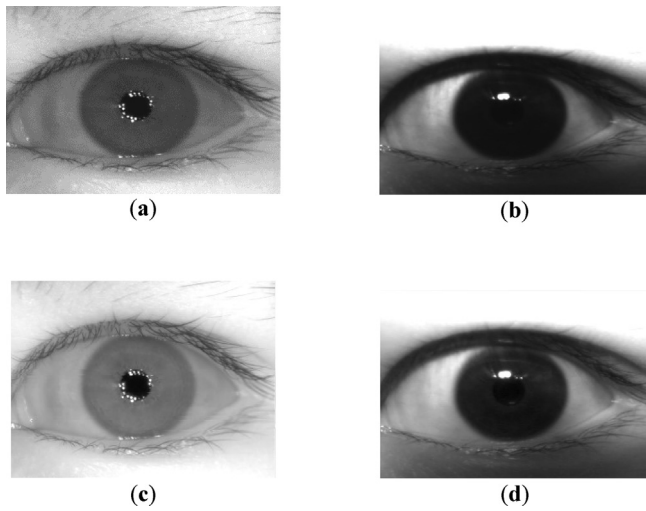


Figure 3. Homomorphic filtering is applied to suppress specular reflection and enhance the iris pattern. (a) Iris image in the near-infrared (NIR) spectrum; (b) Iris image in the visible (VIS) spectrum; (c) NIR iris image after applying homomorphic filtering; (d) VIS red channel iris image after applying homomorphic filtering. (iris image source: PolyU iris database [47]).

2. The Fourier transform is applied to the logarithmic image:

$$I_F = FFT(I_{log}) \tag{2}$$

3. The image in the frequency domain is convolved with a filter, R, that reduces the low frequency components and amplifies the high frequency components:

$$I_R = R * I_F \tag{3}$$

4. An inversed Fourier transform of the filtered images is performed:

$$I_{inv} = FFT^{-1} I_R \tag{4}$$

5. The final image (I_{out}) is obtained by taking the exponential of the result:

$$I_{out} = exp(I_{inv}) \tag{5}$$

3.2. Iris segmentation and normalization

The second step in cross-spectral iris recognition is to localize the iris and pupil boundaries in the NIR and VIS images to obtain the valid iris area that contains information of the iris texture. Table 2 indicates the comparison of various iris segmentation methods. We evaluated four segmentation methods, namely Daugman Integro Operator (DIO), Circular Hough Transform (CHT), Markov Random Field (MRF), and Active Contour. We use 209 NIR iris images and 209 VIS iris images. The successful iris segmentation method is highlighted with the bold text in Table 2. The CHT segmentation method results in the more successful segmented iris images with a ratio of 80% for both NIR and VIS iris

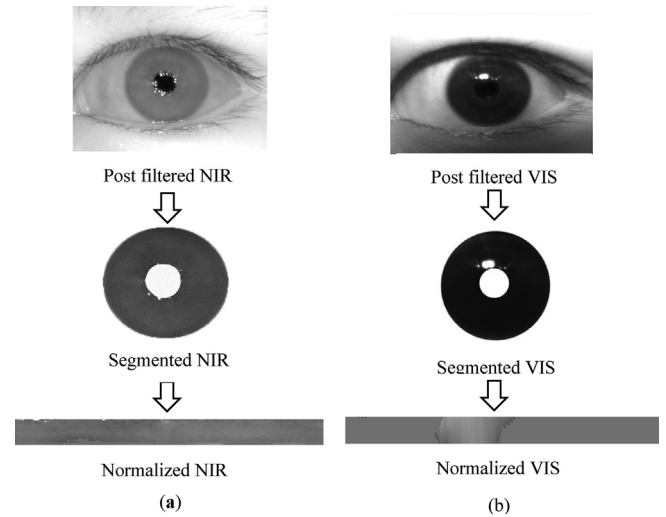


Figure 4. Iris segmentation and normalization processes. (a) Near-infrared (NIR) segmentation and normalization; (b) Visible (VIS) segmentation and normalization. (iris image source: PolyU iris database [47]).

images. DIO and MRF methods failed to segment the VIS iris images while the active contour method failed in the NIR iris images. Therefore, the CHT was used in this study. Figure 4 illustrates the iris segmentation and normalization processes. First, edge maps of the NIR and VIS images were generated from I iris image using canny edge detection. Then, limbic and pupil boundaries were computed by biasing the gradient of I in the vertical direction and weighting the vertical and horizontal gradients equally. The range of the iris radius and pupil radius can be set manually [38]. It should be noted that in the PolyU database, the iris radius is set from 90 to 150 pixels, and the pupil radius set from 28 to 75 pixels.

We then calculated the center of the coordinates of I, the coordinates center of the pupil, the pupil radius, and the iris radius using the Hough transform. First, we computed the limbic boundary and then the pupil boundary in the iris area, as follows [39]:

$$H(x_c, y_c, r) = \sum_{j=1}^n h(x_j, y_j, x_c, y_c, r) \tag{6}$$

In the above equation,

$$h(x_j, y_j, x_c, y_c, r) = \begin{cases} 1, & \text{if } g(x_j, y_j, x_c, y_c, r) = 0 \\ 0, & \text{otherwise.} \end{cases} \tag{7}$$

Where x_c and y_c are the centre coordinates of I, r is the radius of I, and x_j, y_j represent the edge points, for $j = 1, 2, \dots, n$.

Parameter g represents the following:

$$g(x_j, y_j, x_c, y_c, r) = (x_j - x_c)^2 + (y_j - y_c)^2 - r^2 \tag{8}$$

After the center coordinates are obtained, the eyelids are isolated using the Radon transform, and the eyelashes are isolated using a simple thresholding method. Finally, a segmented iris image (I_s) is obtained. Then, the segmented iris image is transformed into given fixed dimension to prepare it for the feature extraction process [40]. In this study,

Table 2. Comparison of successful iris segmentation methods.

Segmentation Methods	NIR	VIS	Segmentation Ratio
Daugman Integro Operator [37]	Success	Failed	50%
Circular Hough Transform [38]	Success	Success	80%
Markov Random Field [38]	Success	Failed	50%
Active Contour [38]	Failed	Success	60%

Daugman's rubber sheet normalization was used. This method transforms the segmented iris area from cartesian coordinates to polar coordinates (r, θ) using the method in [41, 42], as follows:

$$I_s(x(r, \theta), y(r, \theta)) \rightarrow I_N(r, \theta)$$

$$x(r, \theta) = (1 - r)x_p(\theta) + rx_i(\theta)$$

$$y(r, \theta) = (1 - r)y_p(\theta) + ry_i(\theta) \quad (9)$$

where:

$$x_p(\theta) = x_{p0}(\theta) + r_p \times \cos(\theta)$$

$$y_p(\theta) = y_{p0}(\theta) + r_p \times \sin(\theta)$$

$$x_i(\theta) = x_{i0}(\theta) + r_i \times \cos(\theta)$$

$$y_i(\theta) = y_{i0}(\theta) + r_i \times \sin(\theta)$$

here, $I_s(x, y)$ is the segmented iris, (x, y) and (r, θ) are the cartesian coordinates and polar coordinates, respectively. Besides, x_p, y_p are represent the coordinates of the pupil along the θ direction, while x_i, y_i are the iris boundaries in the θ direction. Following the normalization stage, the normalized iris image has a fixed dimension with 20×240 pixels. Figure 5 illustrates the successful and failed segmentation for the NIR and VIS images.

3.3. Phase-based image matching

Phase-based image matching uses the phase information of the 2D DFT of images to match different images. An image consists of a phase and an amplitude. The amplitude is the real part of the fast Fourier transform (FFT) of the image, while the phase is the imaginary part. The height of the correlation peak determines the similarity between two iris images, and the location of the correlation peak indicates the translational image shifts [27]. Phase-based image matching can be divided into several steps [35], as follows:

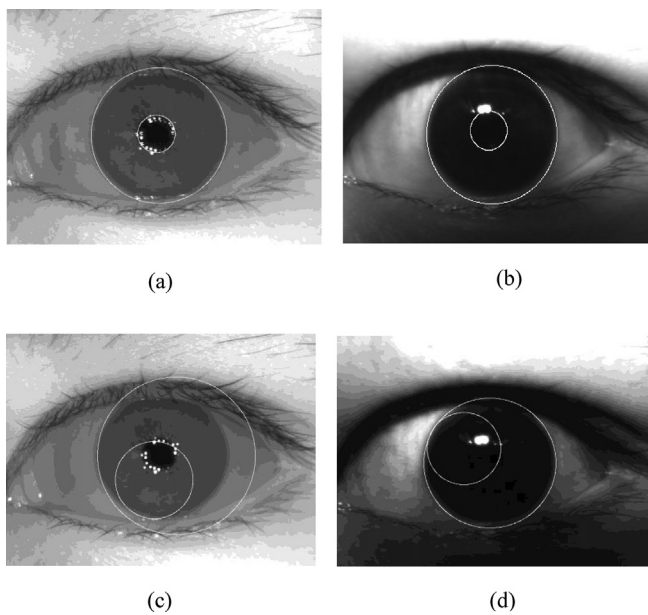


Figure 5. The successful and failed iris segmentation. (a) Successful NIR iris segmented; (b) Successful VIS iris segmented; (c) Failed NIR iris segmented; (d) Failed VIS iris segmented. (iris image source: PolyU iris database [47]).

a. Phase-only correlation (POC) function

POC utilizes information from both low and high frequencies contained in the iris images. In Figure 6, the stage of POC computation is presented. Let two iris images $p(n_1, n_2)$ and $q(n_1, n_2)$, have size $N_1 \times N_2$. The index of the image ranges between $-M_1 \leq n_1 \leq M_1$ ($M_1 > 0$), and $-M_2 \leq n_2 \leq M_2$ ($M_2 > 0$). Thus, $N_1 = 2M_1 + 1$ and $N_2 = 2M_2 + 1$. The 2D DFT of the two images are denoted $P(k_1, k_2)$ and $Q(k_1, k_2)$ respectively, where $-M_1 \leq k_1 \leq M_1$ ($M_1 > 0$), and $-M_2 \leq k_2 \leq M_2$ ($M_2 > 0$). Therefore, $P(k_1, k_2)$ and $Q(k_1, k_2)$ are given as follows [43]:

$$P(k_1, k_2) = \sum_{n_1=-M_1}^{M_1} \sum_{n_2=-M_2}^{M_2} p(n_1, n_2) W_{N_1}^{k_1 n_1} W_{N_2}^{k_2 n_2} = A_P(k_1, k_2) e^{j\theta_P(k_1, k_2)} \quad (10)$$

$$Q(k_1, k_2) = \sum_{n_1=-M_1}^{M_1} \sum_{n_2=-M_2}^{M_2} q(n_1, n_2) W_{N_1}^{k_1 n_1} W_{N_2}^{k_2 n_2} = A_Q(k_1, k_2) e^{j\theta_Q(k_1, k_2)} \quad (11)$$

here, $A_P(k_1, k_2)$ and $A_Q(k_1, k_2)$ are the amplitude components of images p and q, respectively, while $\theta_P(k_1, k_2)$ and $\theta_Q(k_1, k_2)$ are the phase component of images p and q, respectively. In addition, $W_{N_1} = e^{-j\frac{2\pi}{N_1} k_1 n_1}$ and $W_{N_2} = e^{-j\frac{2\pi}{N_2} k_2 n_2}$. The phase difference between $P(k_1, k_2)$ and $Q(k_1, k_2)$ is calculated using the normalized cross-spectrum $R_{PQ}(k_1, k_2)$. The cross-spectrum is a measure of the similarity of two functions as a function of a time shift t. The cross-spectrum $R_{PQ}(k_1, k_2)$ is computed as follows:

$$R_{PQ}(k_1, k_2) = \frac{P(k_1, k_2) \overline{Q(k_1, k_2)}}{|P(k_1, k_2) \overline{Q(k_1, k_2)}|} = e^{j\{\theta_P(k_1, k_2) - \theta_Q(k_1, k_2)\}} \quad (12)$$

here, $\overline{Q(k_1, k_2)}$ represents complex conjugate of $Q(k_1, k_2)$. The 2D inverse DFT (IDFT) of $R_{PQ}(k_1, k_2)$ is denoted as the POC function $R_{PQ}(n_1, n_2)$, which is given as follows:

$$R_{PQ}(n_1, n_2) = \frac{1}{N_1 N_2} \sum_{k_1=-M_1}^{M_1} \sum_{k_2=-M_2}^{M_2} R_{PQ}(k_1, k_2) W_{N_1}^{-k_1 n_1} W_{N_2}^{-k_2 n_2} \quad (13)$$

The POC function $R_{PQ}(n_1, n_2)$ results in the Kronecker delta function $\delta(n_1, n_2)$ if $p(n_1, n_2) = q(n_1, n_2)$. If $p(n_1, n_2)$ and $q(n_1, n_2)$ are similar, the POC function results in a distinct sharp peak. If $p(n_1, n_2)$ and $q(n_1, n_2)$ are not similar, the peak is not significant.

b. Band-limited POC (BLPOC) function

In POC computation, because the high frequency components are emphasized by the POC function $R_{PQ}(n_1, n_2)$, the correlation peak can be decreased even if the two iris images are similar. Therefore, to obtain the maximum correlation peak, the band frequency is limited to a specific area [43]. As illustrated in Figure 7, the most important phase spectrum information is provided only in the significant range (from $-F_1$ to F_1 and from $-F_2$ to F_2). The BLPOC can compute similarity using the range of the inherent frequency band (from $-F_1$ to F_1 and from $-F_2$ to F_2) of the iris texture, where $0 \leq F_1 \leq M_1$ and $0 \leq F_2 \leq M_2$. The effective area of the frequency spectrum is thus represented by $L_1 = 2F_1 + 1$ and $L_2 = 2F_2 + 1$. The BLPOC function is computed as follows [35]:

$$R_{PQ}^{F_1, F_2}(n_1, n_2) = \frac{1}{L_1 L_2} \sum_{k_1=-F_1}^{F_1} \sum_{k_2=-F_2}^{F_2} R_{PQ}(k_1, k_2) W_{L_1}^{-k_1 n_1} W_{L_2}^{-k_2 n_2} \quad (14)$$

here, $-F_1 \leq n_1 \leq F_1$ and $-F_2 \leq n_2 \leq F_2$. The BLPOC function $R_{PQ}^{F_1, F_2}(n_1, n_2)$ produces a maximum peak if the $p(n_1, n_2)$ and $q(n_1, n_2)$ are similar, this value is always normalized to 1. In this study, we used $-F_1 = 8$,

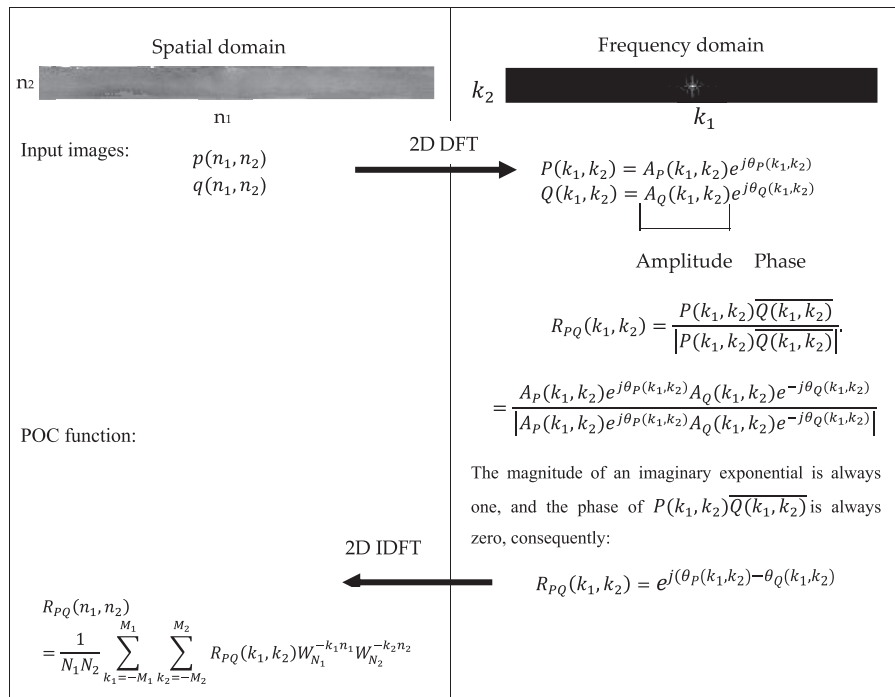


Figure 6. The POC computation.

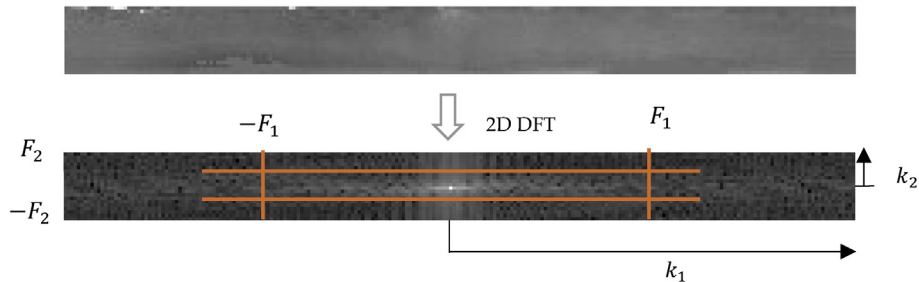


Figure 7. Frequency band of the iris spectrum, which is limited to the significant range (from $-F_1$ to F_1 and from $-F_2$ to F_2). DFT: discrete Fourier transform.

$F_1 = 13$, and $-F_2 = 100$, $F_2 = 140$. These parameters were experimentally selected for an iris template with dimensions of 20×240 .

3.4. Matching decision

Cross-spectral phase-based iris recognition performance is determined via the EER and the ROC curve. The EER summarizes performance with a single number, while the ROC curve uses various scales. The EER signifies that the false acceptance rate (FAR) is equal to the false rejection rate (FRR). The FAR represents an error in which a non-authentic candidate (impostor) is erroneously accepted as an authentic (genuine) user because the matching score exceeds a given threshold. Similarly, the FRR represents an error in which an authentic user is erroneously rejected because the matching score is lower than the threshold. A lower EER characterizes an effective recognition system [44].

The ROC curve, in contrast, is the ratio between the genuine acceptance rate (GAR) and the FAR. The GAR is the rate of an authentic user being correctly accepted when the matching score exceeds the threshold. A ROC curve characterizes effective iris recognition systems placed close to the top of the graph for various FAR values [45, 46].

4. Experimental results and discussions

The experiment was carried out using the PolyU Iris Database [47], which has been provided by The Hong Kong Polytechnic University

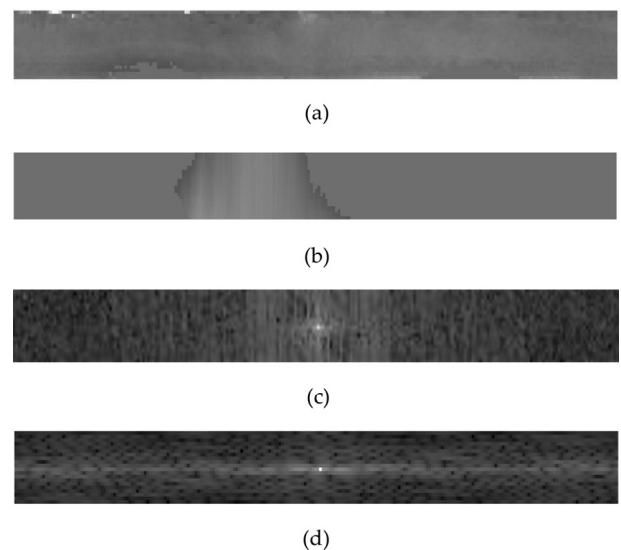


Figure 8. 2D discrete Fourier transform (DFT) spectrum of images in the near-infrared (NIR) spectrum and visible (VIS) spectrum. (a) Normalized NIR iris image; (b) Normalized VIS iris image; (c) 2D DFT spectrum of an image in the NIR spectrum; (d) 2D DFT spectrum of an image in the VIS spectrum.

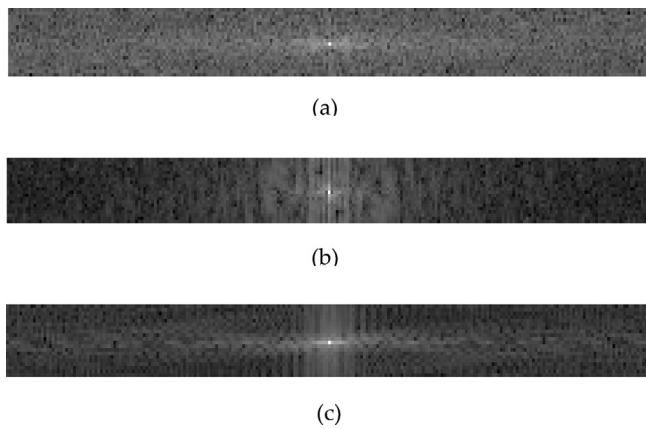


Figure 9. Effect of photometric normalization techniques on 2D discrete Fourier transform (DFT) spectrum. (a) 2D DFT spectrum of visible (VIS) spectrum using TanTriggs filtering; (b) 2D DFT spectrum of VIS spectrum using DCT filtering; (c) 2D DFT spectrum of VIS spectrum using homomorphic filtering.

Cross-Spectral Iris Images Database for research purpose. The use and publication of this data is permitted and ethical under the terms outlined by the provider. The database consists of data from 209 subjects, and the iris images were acquired in the NIR and VIS wavelengths from the left and right eyes. For each subject, there were 15 right-eye images and 15 left-eye images. In total, there were 12,540 iris images with dimensions of 640 × 480. All images in this database were captured using simultaneous bi-spectral imaging, as described in [11].

The experiment was performed using the same algorithm used in reference [48] and [49], using 12000 iris images with a dimension of 20 × 240 from 20 subjects. A total of 20 NIR images of one eye pattern were randomly selected for testing, while 600 VIS images of all the other eye patterns used for training. The total number of genuine comparisons was 600, and the total impostor comparisons were 11,400.

4.1. Homomorphic filtering performance

As previously noted in Section 3, the performance of phase-based cross-spectral iris matching is affected by specular reflection because different illumination conditions between NIR and VIS iris images produce different iris images for the same individual. The 2D DFT spectrum differs for images in the NIR spectrum and images in the VIS spectrum because specular reflection affects the direction of the 2D DFT spectral distribution. Figure 8 presents the 2D DFT spectrum of images in the NIR and VIS spectra. In the NIR spectrum, the distribution of the DFT spectrum is in both the horizontal and vertical directions.

The high frequency can be seen in the middle of the spectrum, while the low frequency is distributed around the center of the coordinate. In the VIS spectrum, the distribution of the DFT spectrum of the iris image is in the horizontal direction. To overcome these drawbacks, we employed photometric normalization techniques prior to the segmentation stages.

We investigated three filtering techniques to eliminate specular reflection: homomorphic filtering, DCT-based filtering, and TanTriggs filtering. Figure 9 demonstrates the effect of photometric normalization on the DFT spectrum of the NIR and VIS iris images. As illustrated, by applying the photometric normalization techniques, the directions of the NIR and VIS spectrum distributions became slightly more similar to each other.

Of the normalization techniques, homomorphic filtering resulted in the best DFT spectrum representation, providing the most similar NIR and VIS spectrum distributions. By suppressing the low-frequency components and amplifying the high-frequency components, homomorphic filtering was able to enhance the iris features and flatten the lighting variations of an image.

Table 3 presents the POC matching scores without filtering and with homomorphic filtering, DCT-based filtering, and TanTriggs filtering. Four test NIR iris images and five training VIS iris images were used, and a match occurred if the POC score was highest for the corresponding pairs. The bold text in Table 3 indicates the highest POC scores which are considered as matching decision. Three successful matches occurred using homomorphic filtering, but only two successful matches occurred

Table 3. POC matching score between NIR and VIS images using no filtering, homomorphic filtering, DCT-based filtering, and TanTriggs filtering.

	NIR 1				NIR 2				NIR 3				NIR 4			
	NF	Homo	DCT	TanTriggs	NF	Homo	DCT	TanTriggs	NF	Homo	DCT	TanTriggs	NF	Homo	DCT	TanTriggs
VIS 1	0.1069	0.1576	0.0633	0.0603	0.0952	0.0585	0.0740	0.0574	0.0788	0.0669	0.0715	0.0505	0.0603	0.0615	0.0599	0.0592
VIS 2	0.0824	0.0723	0.0641	0.0546	0.1016	0.1626	0.0689	0.0589	0.0686	0.0744	0.0673	0.0616	0.0670	0.0540	0.0644	0.0478
VIS 3	0.0953	0.0961	0.1139	0.0555	0.1143	0.0853	0.0593	0.0565	0.0789	0.1937	0.0616	0.0760	0.0739	0.0808	0.0647	0.0579
VIS 4	0.1239	0.0998	0.0830	0.0615	0.1670	0.0803	0.0664	0.0546	0.1054	0.0900	0.0613	0.0634	0.0925	0.0714	0.0620	0.0646
VIS 5	0.1120	0.1156	0.0742	0.0569	0.1368	0.1075	0.0681	0.0535	0.1057	0.1259	0.0656	0.0650	0.0641	0.0689	0.0875	0.0538
Decision	NM	M	NM	NM	NM	M	NM	M	NM	M	NM	M	NM	NM	NM	NM

Table 4. BLPOC matching score between NIR and VIS images using no filtering, homomorphic filtering, DCT-based filtering, and TanTriggs filtering.

	NIR 1				NIR 2				NIR 3				NIR 4			
	NF	Homo	DCT	TanTriggs												
VIS 1	0.313	0.334	0.232	0.220	0.279	0.194	0.201	0.157	0.301	0.176	0.233	0.235	0.253	0.203	0.189	0.178
VIS 2	0.223	0.180	0.190	0.175	0.190	0.369	0.178	0.187	0.213	0.190	0.195	0.203	0.270	0.178	0.189	0.238
VIS 3	0.362	0.210	0.213	0.169	0.335	0.220	0.187	0.232	0.254	0.240	0.189	0.219	0.257	0.179	0.193	0.166
VIS 4	0.445	0.240	0.188	0.179	0.427	0.199	0.195	0.193	0.298	0.172	0.260	0.235	0.196	0.268	0.166	0.219
VIS 5	0.330	0.201	0.173	0.221	0.468	0.189	0.226	0.173	0.266	0.207	0.207	0.182	0.170	0.216	0.168	0.158
Decision	NM	M	M	NM	NM	M	NM	NM	NM	M	NM	NM	NM	M	NM	NM

Note:
Homo: Homomorphic filtering.
NF: No filtering.
NM: No match.
M: Match.

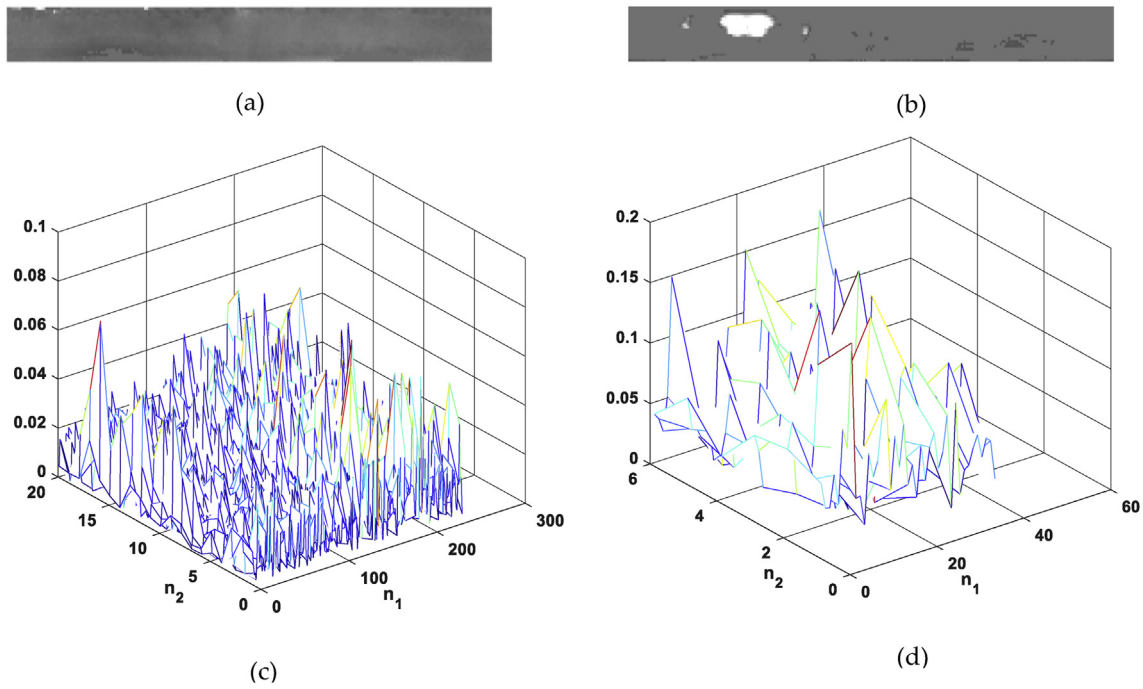


Figure 10. Phase-only correlation (POC) and band-limited phase-only correlation (BLPOC) functions using Homomorphic filtering for impostor matching. (a) Near-infrared iris image; (b) Visible iris image; (c) Impostor matching using POC; (d) Impostor matching using BLPOC.

using TanTriggs filtering. There were no successful matches when no filtering was used or when DCT-based filtering was used; in these cases, the impostor matching scores were higher than the genuine matching scores.

Table 4 illustrates the effects of homomorphic filtering, DCT-based filtering, and TanTriggs filtering on BLPOC matching performance. With homomorphic filtering, all NIR iris images were successfully matched with authentic VIS iris images in four attempts. Here, the genuine images generated higher BLPOC matching scores than the impostor matching scores as noticeable with bold text in Table 4. Unlike

POC, homomorphic filtering significantly increased the BLPOC matching scores. Therefore, homomorphic filtering provides a higher discrimination capability for the BLPOC function than for the POC function.

With DCT-based filtering, there was only one successful match, and nearly all impostor matching scores were higher than the genuine matching scores. Using TanTriggs filtering and no filtering, there were no successful matches. Here, all impostor matching scores were higher than the genuine matching scores. Hence, the homomorphic filtering outperformed other techniques in eliminating specular reflection problem.

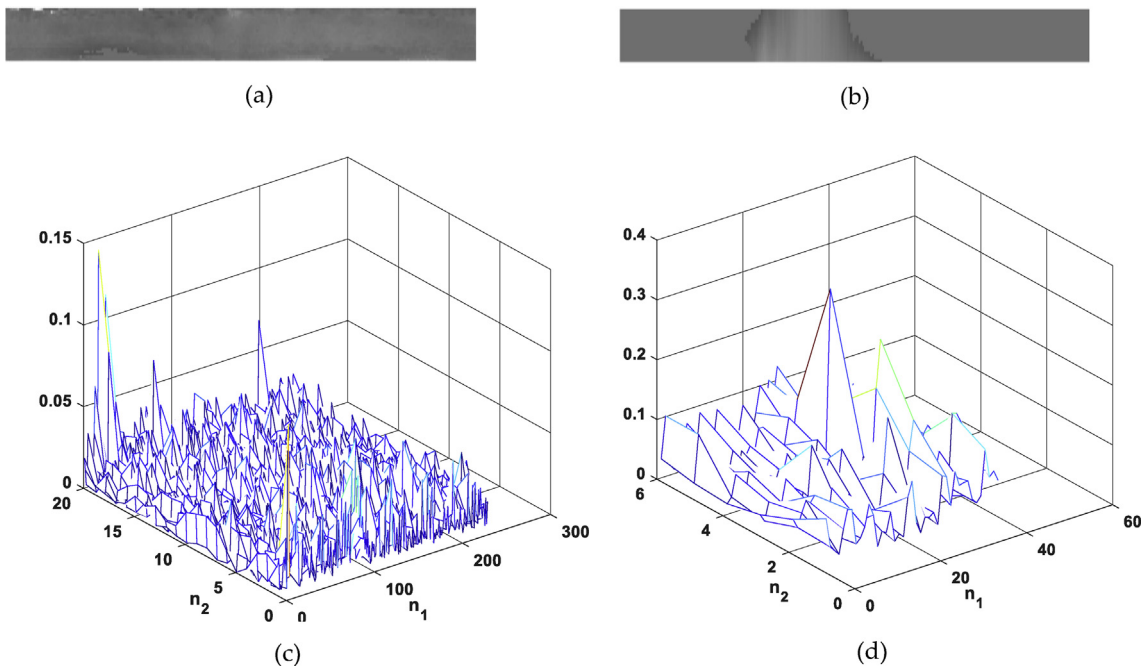


Figure 11. Phase-only correlation (POC) and band-limited phase-only correlation (BLPOC) functions using homomorphic filtering for genuine matching. (a) Near-infrared iris image; (b) Visible iris image; (c) Genuine matching using POC; (d) Genuine matching using BLPOC.

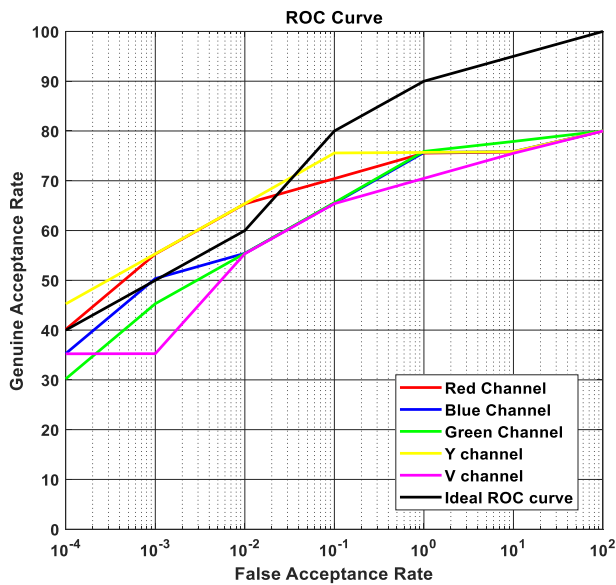


Figure 12. Receiver operating characteristic (ROC) curves using phase-only correlation (POC) for red, green, blue, Y, and V color spaces.

4.2. Matching performance

Figure 10 presents several examples of POC and BLPOC functions using homomorphic filtering for impostor matching. There were no meaningful correlation peaks for either POC and BLPOC functions because the two iris images were not similar. However, in the genuine matching case, the POC and BLPOC functions provided more discriminative correlation peaks, as illustrated in Figure 11; here, BLPOC produced a higher peak than the POC function.

This result was due to selecting only a limited frequency band in computing the BLPOC. Only relevant information was used in the matching process, resulting in a sharp and distinct correlation peak.

Figure 12 illustrates the performance of the POC for red, green, blue, Y, and V color spaces with a variation threshold. A reference threshold of 0.285 was used for the EER. The performance of POC for red, green, blue, Y, and V color spaces was slightly lower than ideal ROC curve. POC resulted in a 75% GAR and a 1% FAR for red, green, blue, and Y color spaces. In contrast, ideal ROC curves result in a 90% GAR. The V color space provided a 70% GAR and a 1% FAR.

BLPOC achieved better performance than POC, as illustrated in Figure 13. For nearly all color channels, BLPOC resulted in superior recognition performance with a 95% GAR and a 1% FAR. Even with a FAR of 0.0001%, BLPOC was able to surpass the ideal ROC curve with a GAR of only 40%; here, BLPOC was able to achieve 50% GAR for all color channels. These results indicate that BLPOC demonstrated superior performance in detecting the similarity between the NIR and VIS iris images. Because the POC peak value was lower than the BLPOC peak value, the performance of POC was lower than that of BLPOC for the same reference threshold.

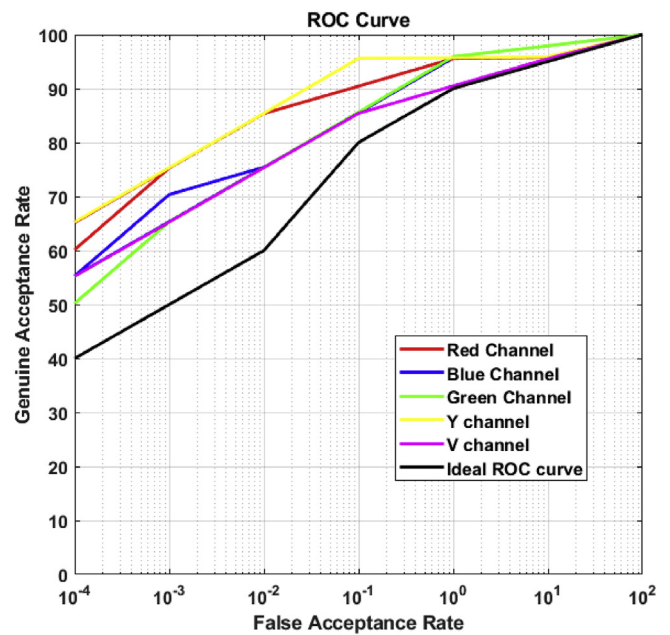


Figure 13. Receiver operating characteristic (ROC) curves using band-limited phase-only correlation (BLPOC) for red, green, blue, Y, and V color spaces. BLPOC results in superior performance for most channels, with a 95% genuine acceptance rate and a 1% false acceptance rate.

Table 5 indicates that phase-based image matching was successful and demonstrated promising performance in the cross-spectral domain. POC and BLPOC produced a GAR of greater than 90% and lower EERs for nearly all color channels. The best recognition performance was achieved for the Y channel (pointed with bold text in Table 5), as it preserved all iris information that was available in the VIS iris images. The Y channel was also less affected by specular reflection, as the light intensity of the color was encoded nonlinearly. In addition, the Y channel was compatible with homomorphic filtering computation.

4.3. Performance comparison with baseline approaches

As described in Table 6, we performed a comparison between the performance of our proposed phase-based technique and existing baseline approaches in the cross-spectral domain. Our proposed cross-spectral iris recognition method outperformed the baseline approaches with an EER of less than 5%. The pioneer cross-spectral iris recognition proposed by Ramaiah and Kumar [11] resulted in an EER about 34.01%. In 2017, Nalla and Kumar [13] improved the cross-spectral performance by proposing a classification framework based on Naive-Bayes Nearest-Neighbor (NBNN) domain adaptation with an EER of 26.68%. The block-based cross-spectral iris recognition method proposed in [31] produced EER with a value of 31.08%, as this method was unable to preserve the correlated information contained in both the NIR and VIS images. The statistical approach [30] and structural approach [29]

Table 5. Performance of near-infrared-visible (NIR-VIS) iris matching using phase only correlation (POC) and band limited phase only BLPOC for different color channels with a high genuine acceptance rate (GAR) and a low equal error rate (EER) with a reference threshold of 0.285.

Color space	POC		BLPOC	
	GAR	EER	GAR	EER
Red channel	85.00	5.00	92.27	0.60
Green channel	85.08	4.93	95.30	0.97
Blue channel	85.00	4.98	95.43	0.10
Y channel	85.09	4.91	95.40	0.59
V channel	85.09	4.90	95.34	0.25

Table 6. Performance comparison of several cross-spectral iris recognition methods. EER: equal error rate.

Matching Method	EER (%)
Ramaiah & Kumar [11]	34.01
Nalla & Kumar [13]	26.68
Statistical based [30]	6.81
Structural based [29]	17.90
Block based [31]	31.08
CNN based [32]	5.39
Proposed Phase based	0.59

produced EERs of 6.8% and 17.9%, respectively. The CNN-based method outlined in [32] displayed a favorable performance with an EER of 5.39%. However, the intensive computation required for this approach is a significant drawback.

Our proposed cross-spectral iris recognition method not only provides exceptional performance with an EER of 0.59% as marked with bold text in Table 6, but it is also simple to implement and does not require heavy computational resources. This is possible because the proposed technique uses a simple iris representation from the phase component of the 2D DFT spectrum. In addition, the proposed framework is suitable for poor-quality iris images, as demonstrated using the PolyU dataset. Using BLPOC and homomorphic filtering, our proposed method significantly improved the performance of cross-spectral iris recognition for NIR and VIS iris image.

5. Conclusions

In this study, we proposed a cross-spectral iris recognition method using phase-based matching and homomorphic filtering to enhance recognition performance. The experimental results demonstrated that the performance of the proposed framework using a VIS-NIR dataset was the highest among the baseline approaches considered in the study, with an EER of 0.59%. The critical aspect of our cross-spectral phase-based matching approach involves homomorphic filtering, which is capable of suppressing illumination. However, the proposed framework was not effective for images that have non-linear intensity variations. In this case, it is hard to obtain the phase correlation between NIR and VIS iris images. In future work, we plan to further improve the performance of cross-spectral iris recognition by combining the BLPOC and POC matching scores with Gradientface-based normalization and developing a more robust algorithm.

Declarations

Author contribution statement

Maulisa Oktiana: Performed the experiments; Analyzed and interpreted the data; Wrote the paper.

Takahiko Horiuchi, Keita Hirai & Yuwaldi Away: Analyzed and interpreted the data.

Khairun Saddami: Performed the experiments; Contributed reagents, materials, analysis tools or data.

Fitri Arnia: Analyzed and interpreted the data; Contributed reagents, materials, analysis tools or data.

Khairul Munadi: Conceived and designed the experiments; Analyzed and interpreted the data.

Funding statement

This work was supported by the Ministry of Research, Technology, and Higher Education of the Republic of Indonesia under the scheme of Pendidikan Magister menuju Doktor untuk Sarjana Unggul (PMDSU), the Peningkatan Kualitas Publikasi Internasional (PKPI)/Sandwich-like

scholarship 2018 and the LPPM Universitas Syiah Kuala under the scheme of Penelitian Calon Profesor (PCP) 2019.

Competing interest statement

The authors declare no conflict of interest.

Additional information

The iris images used in this paper are obtained from the Hong Kong Polytechnic University Cross-Spectral Iris Images Database, which is available on the website (<https://www4.comp.polyu.edu.hk/~csajaykr/polyuiris.htm>). Data associated with this study has been deposited at The Hong Kong Polytechnic University Cross-Spectral Iris Images Database under the accession number YYY.

References

- [1] M.B. Lee, H.G. Hong, K.R. Park, Noisy ocular recognition based on three convolutional neural networks, *Sensors (Basel)* 17 (2017) 1–26.
- [2] M. Arsalan, H.G. Hong, R.A. Naqvi, M.B. Lee, M.C. Kim, D.S. Kim, C.S. Kim, K.R. Park, Deep learning based Iris segmentation for Iris recognition in visible light environment, *Symmetry* 9 (2017) 1–25.
- [3] D.T. Nguyen, N.R. Baek, T.D. Pham, K.R. Park, Presentation attack detection for Iris recognition system using NIR camera sensor, *Sensors (Basel)* 18 (2018) 1–30.
- [4] D.T. Nguyen, T.D. Pham, Y.W. Lee, K.R. Park, Deep learning-based enhanced presentation attack detection for Iris recognition by combining features from local and global regions based on NIR camera sensor, *Sensors* 18 (2018) 2601.
- [5] C.A. Aguilera, A.D. Sappa, C. Aguilera, R. Toledo, Cross-spectral local descriptors via Quadruplet network, *Sensors (Basel)* 17 (2017) 1–14.
- [6] P. Ricaurte, C. Chilán, C.A. Aguilera-Carrasco, B.X. Vintimilla, A.D. Sappa, Feature point descriptors: infrared and visible spectra, *Sensors (Basel)* 14 (2014) 3690–3701.
- [7] M. Trokielewicz, E. Bartuzi, Paper cross-spectral Iris recognition for mobile applications using high-quality color images, *J. Telecommun. Inf. Technol.* 3 (2016) 91–97.
- [8] A. Jain, P. Flynn, A.A. Ross (Eds.), *Handbook of Biometrics*, Springer US, 2008.
- [9] C.A.A.C. Carassco, Local Feature Description in Cross-Spectral Imagery | Computer Vision Center, Universitat Autònoma de Barcelona, Barcelona, 2017.
- [10] M.S. Hosseini, B.N. Araabi, H. Soltanian-Zadeh, Pigment melanin: pattern for Iris recognition, *IEEE Trans. Instrum. Meas.* 59 (2010) 792–804.
- [11] N.P. Ramaiah, A. Kumar, Advancing cross-spectral Iris recognition research using Bi-spectral imaging. In machine intelligence and signal processing, in: R. Singh, M. Vatsa, A. Majumdar, A. Kumar (Eds.), *Advances in Intelligent Systems and Computing*, Springer India, 2016, pp. 1–10.
- [12] J. Zuo, F. Nicolo, N.A. Schmid, Cross spectral iris matching based on predictive image mapping, in: *Proceedings of the 2010 Fourth IEEE International Conference on Biometrics: Theory, Applications and Systems (BTAS)*; Washington, DC, USA, 2010, pp. 1–5.
- [13] P.R. Nalla, A. Kumar, Toward more accurate Iris recognition using cross-spectral matching, *IEEE Trans. Image Process.* 26 (2017) 208–221.
- [14] P. Wild, P. Radu, J. Ferryman, On fusion for multispectral iris recognition, in: *Proceedings of the 2015 International Conference on Biometrics (ICB)*, 2015, pp. 31–37.
- [15] A. Sequeira, L. Chen, P. Wild, J. Ferryman, F. Alonso-Fernandez, K.B. Raja, R. Raghavendra, C. Busch, J. Bigun, Cross-eyed - cross-spectral Iris/periocular recognition database and competition, in: *Proceedings of the 2016 International Conference of the Biometrics Special Interest Group (BIOSIG)*; Germany, 2016, pp. 1–5.
- [16] A. Sharma, S. Verma, M. Vatsa, R. Singh, On cross spectral periocular recognition, in: *Proceedings of the 2014 IEEE International Conference on Image Processing (ICIP)*, France, Paris, 2014, pp. 5007–5011.
- [17] M. Oktiana, K. Saddami, F. Arnia, Y. Away, K. Munadi, Improved cross spectral Iris matching using Gradientface based normalization, in: *Proceedings of the 2018 International Conference on Electrical Engineering and Informatics (ICELTICS)*, Banda Aceh, Indonesia, 2018, pp. 111–116.
- [18] A.C. Teusdea, G. Gabor, Phase-only correlation in fingerprint database registration and matching, *Seria Fizică* 52 (2008) 93–100.
- [19] K. Ito, T. Aoki, T. Higuchi, H. Nakajima, K. Kobayashi, A fingerprint matching algorithm using phase-only correlation, *IEICE Trans. Fund.* E87-A (2004) 682–691.
- [20] T.C. Wei, B.A.B. Rosdi, FPGA based band-limited phase-only correlation (BLPOC) for finger vein recognition system, in: *Proceedings of the 2012 4th International Conference on Intelligent and Advanced Systems (ICIAS2012)*, IEEE: Kuala Lumpur, Malaysia, 2012, pp. 729–734.
- [21] M.S. Mohd Asaari, S.A. Suandi, B.A. Rosdi, Fusion of band limited phase only correlation and width centroid contour distance for finger based biometrics, *Expert Syst. Appl.* 41 (2014) 3367–3382.
- [22] Y.H. Zhu, W. Jia, L. Ling Feng, Palmprint recognition using band-limited phase-only correlation and different representations | SpringerLink, in: *Emerging Intelligent Computing Technology and Applications*; 5th International Conference on Intelligent Computing, ICIC 2009, Ulsan, South Korea, 2009, pp. 270–277.

- [23] L. Zhang, L. Zhang, D. Zhang, Finger-knuckle-print verification based on band-limited phase-only correlation, in: X. Jiang, N. Petkov (Eds.), *Computer Analysis of Images and Patterns*, 5702, Springer Berlin Heidelberg, Berlin, Heidelberg, 2009, pp. 141–148.
- [24] K. Miyazawa, K. Ito, T. Aoki, K. Kobayashi, H. Nakajima, A phase-based Iris recognition algorithm, in: D. Zhang, A.K. Jain (Eds.), *Proceedings of the Advances in Biometrics*, Springer Berlin Heidelberg, 2005, pp. 356–365.
- [25] F. Arnia, N. Pramita, Enhancement of Iris recognition system based on phase only correlation, *TELKOMNIKA* 9 (2011) 387–394.
- [26] M. Oktiana, F. Arnia, Y. Away, K. Munadi, Features for cross spectral image matching: a survey, *Bull. Electr. Eng. Inf.* 7 (2018) 552–560, 560.
- [27] K. Miyazawa, K. Ito, T. Aoki, An efficient iris recognition algorithm using phasebased image matching, in: *Proceedings of the Proc. Int. Conf. On Image Processing*, 2005.
- [28] M. Oktiana, K. Saddami, F. Arnia, Y. Away, K. Munadi, Improved cross-spectral Iris matching using multi-scale Weberface and gabor local binary pattern, in: *Proceedings of the the 10th International Conference on Electronics, Computers and Artificial Intelligence ECAI-2018*, IEEE, 2018, pp. 1–6.
- [29] N.P. Ramajiah, A. Kumar, On matching cross-spectral periocular images for accurate biometrics identification, in: *Proceedings of the 2016 IEEE 8th International Conference on Biometrics Theory, Applications and Systems (BTAS)*, 2016, pp. 1–6.
- [30] M.A.M. Abdullah, S.S. Dlay, W.L. Woo, J.A. Chambers, A novel framework for cross-spectral iris matching, *IP SJ T Comput. Vis. Appl.* 8 (2016) 9.
- [31] R. Vyas, T. Kanumuri, G. Sheoran, Cross spectral iris recognition for surveillance based applications, *Multimed. Tool. Appl.* (2018).
- [32] K. Wang, A. Kumar, Cross-spectral iris recognition using CNN and supervised discrete hashing, *Pattern Recogn.* 86 (2019) 85–98.
- [33] A. Kumar, *The Hong Kong Polytechnic University Cross-Spectral Iris Images Database*, 2017. Available online <http://www4.comp.polyu.edu.hk/~csajaykr/polyuiris.htm>. (Accessed 1 April 2019).
- [34] K. Ito, T. Aoki, Phase-based image matching and its application to biometric recognition, in: *Proceedings of the 2013 Asia-Pacific Signal and Information Processing Association Annual Summit and Conference*, IEEE: Kaohsiung, Taiwan, 2013, pp. 1–7.
- [35] K. Miyazawa, K. Ito, T. Aoki, K. Kobayashi, H. Nakajima, An effective approach for Iris recognition using phase-based image matching, *IEEE Trans. Pattern Anal. Mach. Intell.* 30 (2008) 1741–1756.
- [36] A.A. Abbas, J. Harbi, Image enhancement by using homomorphic filtering model, in: *Proceedings of the the 1 stInternational Conference on Information Technology (ICoIT'17)*; Iraq, 2017, pp. 335–342.
- [37] J.G. Daugman, High confidence visual recognition of persons by a test of statistical independence, *IEEE Trans. Pattern Anal. Mach. Intell.* 15 (1993) 1148–1161.
- [38] L. Masek, *Recognition of Human Iris Patterns for Biometric Identification*, University of Western Australia, Australia, 2003.
- [39] N.J. Ritter, J.R. Cooper, Locating the iris: a first step to registration and identification, in: *Proc. 9th IASTED International Conference on Signal and Image Processing*, 2003, pp. 507–512.
- [40] E.M. Arvacheh, *Study of Segmentation and Normalization for Iris Recognition Systems*, University of Waterloo, Waterloo, Ontario, Canada, 2006.
- [41] T. Kazakov, *Iris Detection and Normalization*, University of Birmingham, Birmingham, 2011.
- [42] S. Chawla, A. Oberoi, A robust algorithm for Iris segmentation and normalization using Hough transform, *Global J. Bus. Manag. Inf. Technol.* 1 (2011) 69–76.
- [43] M. Miura, S. Sakai, S. Aoyama, J. Ishii, K. Ito, T. Aoki, High-accuracy image matching using phase-only correlation and its application, in: *Proceedings of the 2012 Proceedings of SICE Annual Conference (SICE)*, 2012, pp. 307–312.
- [44] J. Daugman, How iris recognition works, *IEEE Trans. Circ. Syst. Video Technol.* 14 (2004) 21–30.
- [45] R. Vyas, T. Kanumuri, G. Sheoran, P. Dubey, Iris recognition through score-level fusion, in: *Proceedings of the CVIP*, 2017, pp. 25–35.
- [46] D.P. Delacrétaz, G. Chollet Bernadette Dorizzi, *Guide to Biometric Reference Systems and Performance Evaluation*, Springer Berlin Heidelberg, 2009.
- [47] *The Hong Kong Polytechnic University Cross-Spectral Iris Images Database*, Aug. 2018 [online] Available: <http://www4.comp.polyu.edu.hk>.
- [48] L. Masek, P. Kovesi, *Matlab Source Code for a Biometric Identification System Based on Iris Patterns*, 2, The School of Computer Science and Software Engineering, The University of Western Australia, 2003 no. 4.
- [49] M. Oktiana, K. Saddami, F. Arnia, yuwaldi Away, K. Hirai, T. Horiuchi, K. Munadi, Advances in Cross-Spectral Iris Recognition Using Integrated Gradientface-Based Normalization, *IEEE Access* 7 (2019) 130484–130494.